Fuel 367 (2024) 131464

Contents lists available at ScienceDirect

Fuel

journal homepage: www.elsevier.com/locate/fuel

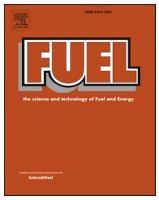

Full Length Article

Reduced kinetics of NH_3/n-heptane: Model analysis and a new small mechanism for engine applications

Vladimir A. Alekseev, Elna J.K. Nilsson *

Division of Combustion Physics, Lund University, Box 118, 22100 Lund, Sweden

ARTICLE INFO

Keywords:
NH_3
N-heptane
Reduced mechanism
Engine
N_2O
Reaction kinetics

ABSTRACT

A compact reduced mechanism covering a wide range of conditions is developed for use in simulations of NH_3/n-heptane combustion in engines. Reduction targets were selected after reviewing available experimental studies of NH_3 combustion in engines. Ignition, flames and oxidation of NH_3/n-heptane mixtures were targeted. Particularly, mixtures with very low molar percentage of n-heptane which are important for the applications were considered. They have been observed to have a distinct ignition behavior. Target quantities also included pollutants with a goal to account for two possible mechanisms of N_2O formation in engines, discussed in literature. The reduced mechanism of this study was developed with ant colony reduction method. It consists of 57 species and 159 reactions, and its range of applicability is 10–100 atm pressure and 0–100 % NH_3 in the fuel mixture. The performance of the mechanism was found comparable to larger models from literature. Importance of carbon–nitrogen interactions, influence of key reactions in the NH_3 subset and effect of CO on N_2O formation were analyzed and discussed in terms of the predictive ability of the reduced mechanism of the present study and those available from literature.

1. Introduction

In recent years ammonia (NH_3) has become widely considered as a potential fossil free energy carrier, suitable for energy storage and power generation [1]. In combustion research NH_3 was previously seen mainly as an intermediate in combustion of fuels with bound nitrogen [2], but now the research focus is shifting towards the use of NH_3 as a standalone fuel or in mixtures with other fuels. Different aspects related to the use of NH_3 as fuel in internal combustion engines (IC engines) and gas turbines have been reviewed in [3,4]. While early research focused mainly at the very possibility of a successful operation of an IC engine with NH_3, since about 2020, a number of studies have explored NH_3 combustion over a broad range of parameters and examined their effect on engine efficiency and pollutant formation. Aspects studied are, for example, engine load, type and amount of the pilot fuel, and injection strategy. Table 1 presents a comparative overview of these studies.

Due to slow ignition of NH_3, running an IC engine on neat NH_3 is challenging, but there exist some recent successful demonstrations [5,6], which implement spark-assisted compression ignition [5] or pre-chamber turbulent jet ignition [6]. The majority of other recent works implemented a dual-fuel strategy with various secondary fuels: hydrogen [7–10], natural gas [11–13], dimethyl ether (DME) [14,15], n-heptane [16], diesel [17–25] or biodiesel [26], gasoline [27,28], or several of these [29].

In most studies, NH_3 is premixed with air at intake, however, direct injection of NH_3 has been applied by Ryu et al. [27] in a spark-ignition (SI) engine; and in compression-ignition (CI) engines by Kong and co-workers [14,15] who mixed liquid DME and NH_3 before injection, and by Zhang et al. [21] who used two injectors for NH_3 and diesel, respectively.

The amount of NH_3 in the fuel varies greatly in the studies outlined in Table 1.NH_3 content is commonly expressed as NH_3 energy fraction, X^E_{NH3}. About half of the studies considered NH_3 to be primarily a fuel additive, with $X^E_{NH3} \leq 0.5$. A few authors, however, achieved very high values of X^E_{NH3}, in Table 1 listed as energy %: up to 90 % NH_3 [25], 93 % [10] and 98.5 % [16] NH_3.

NH_3-containing mixtures generate nitrous oxide (N_2O) whose global warming potential is about 300 times higher than that of CO_2. A number of studies presented in Table 1 report N_2O emissions [5–7,16–20,24,25,29]. The parameters whose influence on N_2O formation have been analyzed are equivalence ratio (ϕ) [5,7,29]; compression ratio [5,7]; amount of NH_3 or diesel [16–18,24,25]; timing of the main

* Corresponding author.
E-mail address: elna.heimdal_nilsson@fysik.lu.se (E.J.K. Nilsson).

https://doi.org/10.1016/j.fuel.2024.131464
Received 3 January 2024; Received in revised form 7 March 2024; Accepted 11 March 2024
Available online 16 March 2024

[17,19,20,25], pilot [17,18,20,25] and post-injection [17] for CI engines, or spark timing [7] for the SI engine; and the ratio between pilot and main diesel [20,24,25].

The studies summarized in Table 1 span a broad range of conditions and can therefore be expected to result in different levels of pollutant formation, identifying common trends. It was observed that N_2O emission has a negative correlation with ϕ [5,7], even though Liu et al. [29] reported little variation. In addition to that, in all studies where the main ignition timing was varied [17,19,20,25], delaying the injection lead to an increase of N_2O. For other quantities, there is a considerable amount of disagreement between studies.

Niki et al. [17] and Jin et al. [25] observed a positive correlation between NH_3 energy fraction and N_2O, while Førby et al. [16] reported the opposite. However, in all three studies, there was a positive correlation between N_2O and unburned NH_3, and a negative correlation between N_2O and engine thermal efficiency. Niki [18] advanced diesel injection to 45° and 60° BTDC and observed opposite trends in N_2O formation with increasing X^E_{NH3} for these two regimes. Moreover, in both cases the unburned NH_3 and thermal efficiency increased with X^E_{NH3}, contrary to [16,17,25].

Further discrepancies are seen in relation to the time of pilot injection (t_{pre}) and diesel split ratio (DSR). Niki et al. [17] and Jin et al. [25] observed negative correlation between t_{pre} and N_2O, while Yousefi et al. [20] and Niki [18] had the opposite. All of the above studies had positive correlation between N_2O and unburned NH_3, except for Niki et al. [17], who recorded the contrary. Opposite trends between the studies [18,20,25] exist in terms of engine thermal efficiency and N_2O (or unburned NH_3) as well. Similarly, disagreement exists in the effect of DSR on N_2O [20,24,25].

Among the reviewed studies, two distinct explanations to the formation of N_2O are presented. Westlye et al. [7] proposed that N_2O is formed during expansion and exhaust strokes. Unburned NH_3 released from crevice volume is mixed with product NO_x, and N_2O is formed via the selective non-catalytic reduction mechanism (SNCR, or $DeNO_x$). This mechanism was subsequently referred to by Mounaïm-Rousselle et al. [5] and Førby et al. [16]. The second mechanism, advocated by Jin et al. [25] and Mi et al. [24], assumes that N_2O is produced at the flame front and is not immediately consumed due to incomplete (disrupted) combustion. Niki et al. [17] lists both mechanisms as possible pathways for N_2O formation. Several authors discuss correlation between temperature and N_2O, however, both of the described mechanisms, in this work refered to as the "$DeNO_x$" and "disrupted flame" mechanisms, respectively, require low temperature for N_2O to be either produced ($DeNO_x$) or sustained (disrupted flame): SNCR window is ca. 1100–1400 K [2], while any N_2O produced at the flame front would decompose via.

$$N_2O\ (+M) = N_2 + O\ (+M), \tag{R1}$$

if temperature stays sufficiently high (at 1400 K, N_2O would decrease by an order of magnitude within ca. 20 ms, and within ca. 2 ms at 1600 K). Therefore, unless N_2O measurements are performed in-situ, neither of the mechanisms can be disqualified, however, all studies in Table 1 report N_2O from the exhaust.

The disagreement in N_2O formation trends described above suggests that it is sensitive to a variety of operational parameters, and is a complex product of the effects of flow and chemistry. To increase the understanding of N_2O formation, and as a result improve mitigation strategies, the effects can be investigated using computational fluid dynamics (CFD) simulations with explicit chemistry schemes. However, due to limitations in computational capacity the reaction schemes need to be compact, but still accurate in the relevant range of conditions. Diesel fuel, frequently seen as the secondary fuel in experimental studies, is often represented by a surrogate such as n-heptane (C_7H_{16}) in the modeling. Concerning NH_3/n-heptane, there exist several reaction schemes developed for use in CFD, e.g. [30–32]. The two more recent and smaller ones [31,32] contain 67 species and 387 reactions, and 72 species and 495 reactions, respectively (Ar and He not counted, reversible reactions count as 1). These mechanisms are on the upper limit of what can be used in the relevant CFD models. The broad engine operating conditions reviewed above, and the $DeNO_x$ mechanism for N_2O formation were not targeted in development of the existing reduced mechanisms for NH_3/n-heptane.

In the present work, a new reduced scheme is presented, developed for engine-relevant conditions, covering various operational strategies. It also accounts for different pathways for N_2O formation. Combustion and oxidation of NH_3/n-heptane was analyzed using 0D and 1D ideal

Table 1
Overview of experimental studies with NH_3 and different secondary fuels, in IC engines.

Source	Year	Ignition type	Second fuel	NH_3, % energy	NH_3 injection method	Engine speed, RPM (min^{-1})	P_{max}, atm	N_2O meas.
Mounaïm-Rousselle et al. [5]	2021	SA-CI	neat NH_3	100	Premixed	650–2000	40–80	yes
Liu et al. [6]	2023	SI, TJI	neat NH_3	100	Premixed	800	25–40	yes
Westlye et al. [7]	2013	SI	H_2	0–84	Premixed	1000	15–45	yes
Lhuillier et al. [8]	2021	SI	H_2	0–66	Premixed	1500	40–55	no
Pandey et al. [9]	2023	SI	H_2	0–76	Premixed	1800	40–50	no
Pyrc et al. [10]	2023	SI	H_2	30–93	Premixed	600	30–38	no
Oh et al. [12]	2021	SI	natural gas	0–28	Premixed	840	21–27	no
Oh et al. [13]	2022	SI	natural gas	0–20	Premixed	1100	<62	no
Wei et al. [11]	2023	SI	natural gas	0–37	Premixed	1190	45–60	no
Gross and Kong [14]	2013	CI	DME	0–30	Direct	2200–2550	60–75	no
Ryu et al. [15]	2014	CI	DME	0–49	Direct	1900–2500	50–80	no
Førby et al. [16]	2023	CI	n-heptane	80–98	Premixed	1200	~50	yes
Niki et al. [17]	2019	CI	diesel	0–15	Premixed	1362	60–70	yes
Niki [18]	2021	CI	diesel	45	Premixed	1500	80–110	yes
Yousefi et al. [19]	2022	CI	diesel	0–40	Premixed	910	80–90	yes
Yousefi et al. [20]	2022	CI	diesel	0–40	Premixed	910	80–100	yes
Zhang et al. [21]	2023	CI	diesel	0–50	Direct	375	~60	no
Sun et al. [22]	2023	CI	diesel	0–80	Premixed	1000	22–38	no
Wu et al. [23]	2023	CI	diesel	N/A	Premixed	1500	70–75	no
Mi et al. [24]	2023	CI	diesel	40–70	Premixed	1500	80–110	yes
Jin et al. [25]	2023	CI	diesel	0–90	Premixed	1000	70–100	yes
Elumalai and Ravi [26]	2022	CI	biodiesel	0–50	Premixed	1500	40–83	no
Ryu et al. [27]	2014	SI	gasoline	0–78	Direct	1800	15–16	no
Liu et al. [28]	2023	SA-CI	gasoline	0–28	Premixed	1500–2000	60–70	no
Liu et al. [29]	2023	SI-TJI	H_2, CH_4, gasoline	N/A	Premixed	800	20–40	yes

SI – spark ignition; CI – compression ignition; SA-CI – spark-assisted CI; TJI – turbulent jet ignition; N_2O meas. – N_2O measurements reported in source.

reactor models, and the target space for reduction (including pollutants) was thoroughly constructed. During reduction, these 0D and 1D reactors were utilized simultaneously. The performance of the mechanism in engine-relevant conditions is discussed and compared to literature models [31,32].

2. Methods

In this work, the Ant-Colony Reduction (ACR) method developed by Pichler [33] is utilized, in combination with manual steps. The combined methodology is motivated by the challenge to construct a compact dual-fuel mechanism for two fuels with such varying reactivity, and over wide range of conditions.

ACR is a semi-stochastic build-up mechanism generating algorithm with a customizable target function that accommodates multiple reactor models, scalar and vector target quantities, and it generates mechanisms with a very low number of reactions. During reduction, performance in the whole target space acts as feedback to the mechanism-generating algorithm. This marks a difference to a more common approach where mechanisms are tested against a broader target space at the validation stage. The use of multiple reactor geometries during reduction is an advantage compared to, e.g., commercially available reduction package in CHEMKIN [34].

As initial steps before a mechanism reduction, a detailed target mechanism and appropriate reactor models capturing the relevant combustion targets need to be selected. Also, the reduction space must be defined in terms of initial parameters, such as NH_3/n-heptane mixture composition, stoichiometry, temperature, pressure and characteristic time scales. The selected entities must be adequate and relevant to the engine conditions, moreover, the end result is greatly affected by these initial choices, therefore, the selection process is described in detail below.

2.1. Selection of the reactor models

As discussed in Section 1, in IC engines, NH_3 can be either premixed with air at intake or injected directly. Also, diesel fuel might contain a pre- or post-injected component. To accommodate for such different injection strategies, it was decided to target both ignition and flame propagation during reduction stage, by using the closed homogeneous 0D reactor and 1D free-propagating flame, respectively. The corresponding target quantities are ignition delay time (IDT) and laminar burning velocity (LBV).

Additional targets were selected in order to account for the two possible mechanisms of N_2O formation proposed in the experimental studies, i.e., the disrupted flame mechanism and the $DeNO_x$ mechanism. First, the "1D flame" component of the ACR target function was extended with N_2O and NO concentrations. A correct prediction of NO formation is necessary, as NO is a reactant in the $DeNO_x$ mechanism. This process was in turn represented by modeling oxidation of $NH_3/O_2/N_2$ mixtures in presence of NO at high pressures and intermediate temperatures in adiabatic 0D reactors, and N_2O temporal profiles were targeted.

2.2. Selection of the initial mixture parameters

Table 2 contains information on the selected range of initial mixture parameters for each of the three types of reactors used during the reduction process. Range of pressure was determined directly from the literature analysis presented in Table 1. The upper border of the characteristic timescale of $\sim 10^{-1}$ s, which served as the maximal allowed IDT and the oxidation end time, corresponds to 60° CAD piston movement in a slowly operating marine engine ~ 100 RPM. The lower temperature limit of 600 K for ignition cases corresponds to a pressure of ca. 10 atm at the end of compression, and at the same time, to 0.1 s IDT of pure n-heptane at 100 atm (i.e., no ignition faster than 0.1 s is possible below 600 K). The temperature window for the $DeNO_x$ oxidation cases depends on residence time and pressure; therefore, its lower boundary turned out to be somewhat lower than specified in [2] due to higher pressures. For flame simulations, a single elevated temperature of 500 K was selected, a temperature where auto-ignition does not yet occur. One temperature was found to be sufficient since temperature dependence of LBV has a weak dependence on chemistry compared to LBV itself [35].

Table 2
Mixture parameters for each of the implemented reactor models.

reactor type	0D C_v	1D flame	0D C_p
target	IDT	LBV, N_2O, NO	N_2O(t)
time scale, s	≤ 0.1	N/A	≤ 0.1
p, atm	10–100	10–100	10–100
T_0, K	600–1400	500	800–1400
ϕ	0.5–1.5	0.7–1.3	0.6–1
X_{NH3} (mol. %)	0–100 %	0–100 %	100 %
No. cases	553	11	62

C_v and C_p – constant volume and constant pressure reactors, respectively.

Despite that in the majority of the experimental engine studies listed in Section 1, NH_3 is premixed with air at the inlet, the diesel fuel is still injected directly, leading to a variety of local equivalence ratios in the combustion chamber. According to Mastorakos [36], in non-premixed combustion, the stoichiometric mixture fraction is not directly related to the most reactive mixture fraction, and the latter is most often located at the lean side [36]. Therefore, it was decided to vary φ to both lean and rich sides for ignition and flame cases, while for the $DeNO_x$ oxidation it is assumed that NH_3/air ratio cannot exceed stoichiometric (since unburned NH_3 from crevices had to be premixed at inlet).Several experimental studies [10,16,25] achieved a stable engine operation when the energy fraction of NH_3 in the fuel was kept near or above 90 %. When recalculated to mole fractions, more common in kinetic studies, and assuming the second fuel to be n-heptane, it equals 99 %. The two fuel components, NH_3 and n-heptane, have a qualitatively different ignition behavior. Fig. 1 presents IDT of NH_3/n-heptane, calculated with the detailed mechanism by Thorsen et al. [37] and constrained by the upper time limit of 0.1 s, for the complete range of n-heptane mole fractions. As little as 0.5 % n-heptane by mole (7 % by energy) significantly accelerates ignition and affects its temperature dependence, while after about 40 %, the IDT closely resembles pure n-heptane. To preserve such behavior in the reduced mechanism, the reduction target space contained mixtures ranging from 0 % to 100 % n-heptane (specifically, 0,

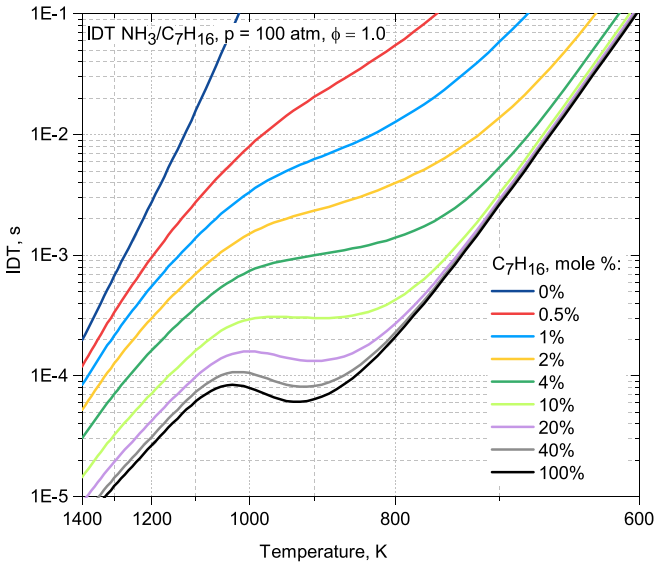

Fig. 1. IDT of stoichiometric NH_3/n-heptane mixtures at 100 atm with varied fraction of n-heptane calculated with the mechanism of Thorsen et al. [37].

0.5, 2, 10, 40 and 100 % by mole).

The influence of the mixture composition on the LBV of NH_3/n-heptane, when expressed in mole fractions, is also non-linear, as evident from the work of Lubrano Lavadera et al. [38]. The dependence becomes quasi-linear if mass fractions are adopted. The kinetic analysis in that work has shown that for LBV no direct chemical coupling effect needs to be considered. As flame simulations are computationally heavy compared to IDT, the target space in the present work is limited to mixtures with 0, 50, and 100 % NH_3 (by mole).

For the $DeNO_x$ N_2O formation, only mixtures without carbon-containing species were considered during reduction, since the oxidation is expected to occur when products (containing NO) mix with the NH_3/air mixture. For the studied conditions, no chemical effects of CO_2 or H_2O were observed in test runs, and the influence of CO will be discussed separately in Section 3. In present work, it was assumed that reaction

$$CO + N_2O = CO_2 + N_2 \quad (R2)$$

has a much slower rate at low and intermediate temperatures than in [37], leading to a more limited chemical effect of CO than was predicted by [37].

The proportions of initial $DeNO_x$ reactants: NH_3, air, the product gas and NO in the real engine simulations are not known a-priori, therefore, for modeling consistency, the amount of the inert component (N_2) in the O_2/N_2 oxidizing mixture was varied, and the concentration of NO was assumed to be 0.1 % by mole.

2.3. Selection of chemical mechanisms

It has been shown that subset of reactions between carbon- and nitrogen-containing species is necessary for representing ignition of binary NH_3-containing fuels (see, e.g., [39–41]). For NH_3/n-heptane, dedicated detailed mechanisms that include interaction subsets were developed only recently [37,42]. Therefore, the reduced mechanism by Wang et al. [32] employed the model of Dong et al. [42] as target, but earlier models by Liu et al. [30] and Xu et al. [31] were developed without considering any interaction chemistry.

In the present study, the mechanism of Thorsen et al. [37] was selected as the target mechanism. This model is based on the continuously updated Glarborg mechanism [2,43] and the detailed n-heptane mechanism of Zhang et al. [44]. The C3-C7 interaction subset [37] was developed with the aim to simulate ignition of NH_3/n-heptane mixtures at 10–15 bar available from [45], and oxidation of these mixtures in jet-stirred and flow reactors at pressures up to 100 bar [37]. The Supplementary Material (SM) contains additional validation for the mechanism [37] against the experiments of [38,42] (Figs. S6,S7). Note that all IDT [42,45] and LBV [38] experimental data for NH_3/n-heptane mixtures is largely outside the target space considered in the present study due to either pressure [38] or type and amount of dilution [42,45]: only one IDT dataset at the lower pressure border (10 atm) and with a rather narrow temperature window from [42] can be considered (see Fig. S6). Therefore, reliability of the predictions of the target mechanism [37] had to be assumed inside the target space of the present study.

Prior to reduction, an intermediate base model was constructed by merging subsets of reactions for n-heptane, NH_3 and their interactions, following the approach of Wang et al. [32]. The n-heptane sub-mechanism of the reduced model [32], which itself is a modified version of the reduced model of Chang et al. [46], was merged with the detailed H/N/O and the C/H/N/O submechanisms of Thorsen et al. [37], keeping the hydrogen submechanism from [37]. As will be discussed in the results section, the rates of the key reactions in the H/N/O sub-mechanism in the base/target mechanisms are a major contributor to the observed differences in the performance of the reduced mechanisms analyzed in the present work, therefore, we rely on most recent updates in the H/N/O subset by Glarborg [43], that were implemented into the target mechanism [37].

The C3-C7 interaction subset was based on the target mechanism [37]. Rates of reactions of the same classes as in [37] were reconstructed for the C3-C7 hydrocarbon species present in [32]. For reactions that required lumping, e.g.

$$C_7H_{16} + NH_2 = C_7H_{15}\text{-i} + NH_3, \quad (R3)$$

where i = 1,2,3,4 denotes one of the four heptyl isomers, forward and reverse channels were entered separately, i.e.:

$$C_7H_{16} + NH_2 => C_7H_{15} + NH_3 \quad (R4)$$

$$C_7H_{15} + NH_3 => C_7H_{16} + NH_2, \quad (-R4)$$

with the forward rate constant being a 3-term fit of the sum of the corresponding rate constants in the temperature range of 300–2500 K, and the reverse rate being a 3-term fit of a weighted sum of the reverse rate constants for the primary and secondary heptyl radicals, with a branching ratio (weight) calculated approximately using the forward rates. Overall, the merged mechanism contained 143 species and 989 reactions.

Some rate constants were optimized or modified to improve the performance of the base mechanism in terms of LBV and IDT, in comparison to the target mechanism [37]. The process is reported in detail in the SM. To improve LBV, three reactions from the C2-C3 subset were modified, and for ignition, A-factors of 18 reactions were optimized. These 18 reactions were either from the C7 fuel breakdown subset of [32,46], where rates are to some extent artificial by design, or from the C/N interaction subset, where many rates were estimated in the present work. These reactions can thus be considered to have large uncertainty limits. With such approach, the full NH_3 submechanism remained intact from the target model [37]. Optimization was performed with the differential evolution algorithm, similar to previous work [47].

The exact reactions for optimization were selected after performing a global sensitivity analysis as described in the SM. All optimized reactions with their rate constants are listed in the SM. The comparison between the base and the target mechanisms can be viewed in Figs. 2-4, where some selected conditions are presented, while the whole target space is reported in the SM. Typically, some discrepancy was observed between the base and target mechanisms even after optimization in terms of IDT at low temperatures (see Fig. 2), especially in mixtures with lowest amount of n-heptane. For LBV, 100 % n-heptane was reproduced

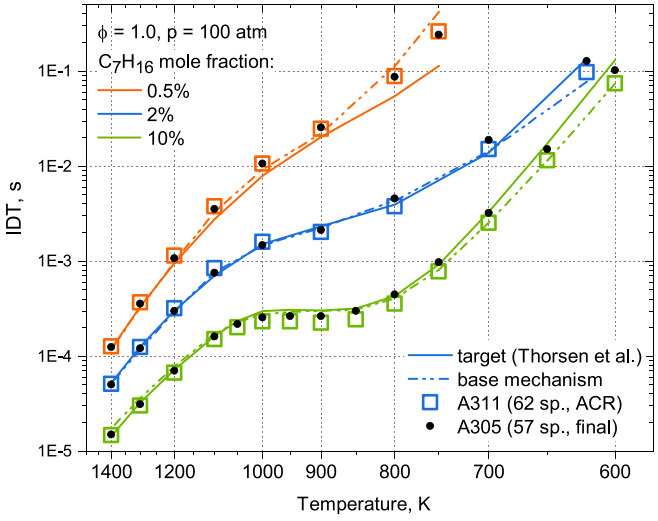

Fig. 2. Ignition delay times for three NH_3/n-heptane mixtures. Solid lines: target mechanism [37], dashed lines: base mechanism, squares: initial 62-species mechanism after ACR reduction (A311); black dots: final 57-species mechanism (A305).

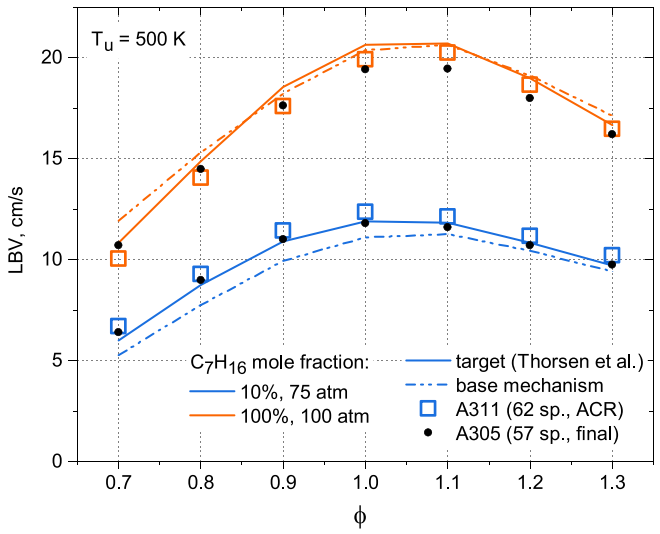

Fig. 3. Laminar burning velocities for NH_3/n-heptane + air. Lines and symbols correspond to same mechanisms as in Fig. 2.

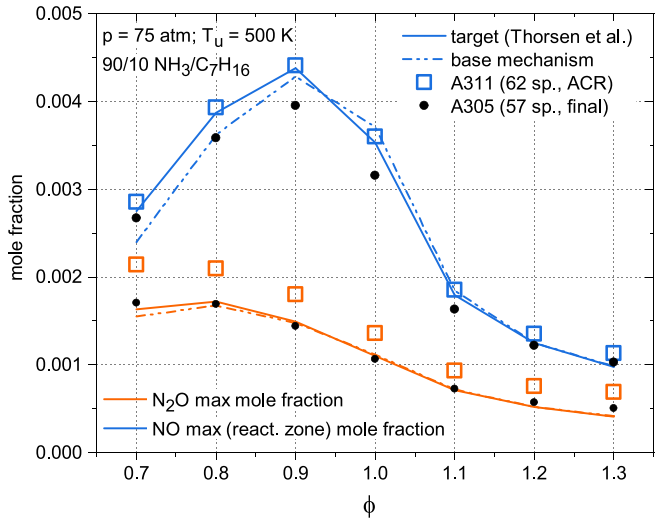

Fig. 4. Maximal (reaction zone) mole fractions of N_2O (orange) and NO (blue). Lines and symbols correspond to same mechanisms as in Fig. 2. (For interpretation of the references to colour in this figure legend, the reader is referred to the web version of this article.)

better than binary mixtures (see Fig. 3 and Fig. S9 in SM). Implementation of the lumped and reduced n-heptane submechanism also affected pathways for NO formation, as can be seen in Fig. 4 and Figs. S11-S13 in SM. Overall, however, the performance of the base model was satisfactory for subsequent reduction.

2.4. Reduction procedure

The ACR Python code [33] has been used previously to obtain reduced mechanisms for high-pressure n-heptane combustion [48]. In the present work, the ant colony ran in a single target space including IDT, LBV, and species profiles in 0D and 1D reactors. Predictions of the detailed mechanism [37] were used as targets, while the starting point for the reduction was the base merged model described above. Several reactions were marked as "important" and forced to be included into all generated mechanisms. A number of reactions from the NO_x subset, which do not belong to major reaction chains, were included manually. The preferred approximate range of sizes of the generated mechanisms can be selected before reduction, this was done after preliminary runs by finding an optimal trade-off between mechanisms' size and their accuracy. The final candidate mechanism was selected from the generated mechanism pool based on the overall averaged accuracy, the average accuracies of each target quantity, maximal deviations from target for each target quantity, and on the mechanism size. The work was focused on determining an optimal set of initial settings to maximize the accuracy of the best ant-generated mechanism, without relying heavily on subsequent optimization as in [48]. Only five rate constants were re-optimized after reduction (see Table S2 in the SM).

The ACR code is integrated with Cantera 2.4.0 [49] Python libraries, while both Cantera and Chemkin 2020 R2 [34] were used for validation and analysis. While less strict solver parameters, e.g., the allowed gradient between grid points for the flame simulations (GRAD) were used during reduction, for figures in this article, the GRAD parameter was set to 0.025 (0.06 for [37] due to its size), resulting in at least 300 grid points. In 0D simulations, the absolute and relative solver tolerances were set to at least 1E-20 and 1E-9, respectively. Ignition was determined at the inflection of the temperature profile. In flames, mixture-averaged formulation of the transport properties was set.

After ACR reduction, a candidate mechanism (A311) with 62 species and 161 reactions was selected. Its performance characteristics are presented in Table 3. Please note than in this table and throughout the paper, accuracy is defined as a sum of absolute mean changes for each target case:

$$A = \frac{1}{n}\sum_{i=1}^{n}\frac{|y_i - y_i^0|}{\max(y_i, y_i^0)} \times 100\%$$

where y_i and y_i^0 are evaluated quantities for the reduced and target models, respectively, and n is a number of targets of the same kind (e.g., IDT or LBV). In case of the overall accuracy, accuracies are weighted over each of the target quantities presented in Table 3. Table S3 in the SM lists all 626 modeling cases that correspond to the target space of Tables 2 and 3 with the corresponding weight functions for each of the target quantity.

The mechanism A311 was further modified and reduced manually, and a few rate constants were optimized, with a goal of achieving smaller size while preserving (or even improving) the overall accuracy. As ACR is a semi-stochastic build-up method, certain reactions important to a smaller subset of targets might be omitted by the algorithm. In addition to that, it is possible to manually remove species while keeping the corresponding reaction pathways by reaction lumping. These manual steps were performed by validating the test versions of the mechanism against the same target space as during the ACR reduction. All manual steps are listed in Table S4 in the SM and are outlined below.

First, to improve performance in terms of N_2O profiles in flames, three reversible reactions were added, which were initially omitted by ACR. Next, few species were further removed, either with all their reactions, or reaction chains were bundled together, eliminating intermediate steps. To ensure compatibility with CFD solvers such as OpenFOAM [50], reactions with pressure dependence through logarithmic interpolation (PLOG) were expressed as pressure-independent. Two PLOG reactions remained in the mechanism after reduction, and only one of them possessed pressure dependence in the 10–100 atm applicability range of the mechanism, that is reaction

$$CO + OH = CO_2 + H \quad (R5)$$

For (R5), rate coefficient at 10 atm was simply taken, as its pressure dependence in the 10–100 atm pressure range was found to be weak.

It was decided to replace rate coefficients of reaction (R2), i.e.

$$CO + N_2O = CO_2 + N_2.$$

added at the first step, to an expression determined by Loirat et al. [51]. This value is implemented in, e.g., the Konnov detailed mechanism [52].

Table 3
Size and performance of the target, intermediate and final mechanisms.

mech.	species	reactions			accuracy, %					
		total	rev.	irrev.	overall	$N2O^{fl}$	NO^{fl}	LBV	IDT	$N2O^{fr}$
target	1367	6314	5228	1086	100	100	100	100	100	100
base	143	989	942	47	92	98	91	98	90	100
A311	62	161	150	11	87	87	91	94	86	86
A305	57	158	145	13	89	95	88	96	89	87

Target: target mechanism [37], base: base mechanism; A311 – after ACR reduction, A305 – final version; (ir)rev. – (ir)reversible; fl – flame; fr – flow reactor ($DeNO_x$ mechanism).

In the target mechanism [37], expression recommended in the review of Tsang and Herron [53] is used. The two rates are similar at high temperatures, however, the difference at ~ 700 K becomes around 10^5, resulting in qualitatively different N_2O predictions for NH_3/NO oxidation cases in presence of CO and before ignition of NH_3/n-heptane mixtures, as shown in Section 3.3 and SM. Since [53], there appeared several studies questioning the preferred rate constant [53]. Wang et al. [54] calculated the activation barriers for a number of direct and indirect transitions, and their values were in agreement with the activation energy of 46 kcal/mol of Loirat et al. [51]. Recently, Krupnov and Pogosbekian [55] calculated potential energies and rate constants for this reaction, and they appeared to be in qualitative agreement with [51], but ~ 200 to 10 times slower at T = 600–2000 K, respectively (see Fig. S3 in SM). Considering that [51] and [53] agree at T ≈ 2000 K, in the present work, an expression from [51] was adopted.

Next, reactions from the previously optimized subset were once again revisited. Five reactions received new rate constants following re-optimization. During the process, the A-factors were allowed to change only in direction that would bring them closer to the corresponding values in the detailed mechanism [37]. Finally, two reactions:

$$HNO + H = NO + H_2 \quad (R6)$$

$$CO + NO_2 = CO_2 + NO \quad (R7)$$

were inserted following additional analyses that will be described in Sections 3.2.2 and Sections 3.3, respectively. Table S4 in the SM lists all manual changes providing details on the rate constants. The final version of the mechanism is presented in Table 3 as A305. It is provided in Chemkin and Cantera formats in the SM.

The applicability range of the mechanism is determined by the target space parameters of Table 2, e.g., pressure range 10–100 atm, NH_3 fractions 0–100 %, NO and N_2O formation etc. One exception that is outside the target space of the present work is NO formation in rich 100 % n-heptane mixtures (see Fig. S13), which are of little practical relevance. The reduced mechanism of the present work is supposed to be used only under conditions listed in Table 2.

Figs. 2-4 illustrate the performance of intermediate versions of the mechanism and its final version at selected conditions, while the whole target space can be found in the SM. Since reduction was performed targeting the detailed mechanism [37], the reduced models were found to be closer to the target mechanism than to the base mechanism at certain conditions. All mechanisms perform qualitatively similar, and quantitative difference was measured by accuracy scores as reported in Table 3. In particular, predictions of N_2O in flames of NH_3/n-heptane mixtures by the A305 mechanism have significantly improved compared to A311 due to addition of reactions, e.g. (R2), as well as

$$NH + NO = N_2 + OH \quad (R8)$$

Reaction (R8) competes with high-temperature formation route of N_2O [2]:

$$NH + NO = N_2O + H \quad (R9)$$

Due to (R8), accuracy of NO predictions has slightly lowered (see Fig. 4), however, since N_2O accuracy has increased to a larger degree, (R8) was kept in the final mechanism.

3. Results

3.1. Composition of the mechanism

The reduced mechanism developed in the present work and literature models [30–32] are intended to be used in CFD, however, they are produced with different methodologies and have different number of species and reactions in their constituent submechanisms, as seen in Table 4. The A305 mechanism is significantly smaller compared to the others, in terms of both reactions and species, while maintaining an overall good accuracy. To understand the differences in performance between the mechanisms, analysis of composition of different reaction subsets is necessary. In the later comparison of modeling results also the difference in size should be considered as a factor when judging the overall performance and usefulness of the A305 mechanism.

The hydrocarbon submechanisms of A305, Xu et al. [31] and Wang et al. [32] are all based on a multi-fuel model of Chang et al. [46], whose size for n-heptane is also listed in Table 4. The model of Xu et al. [31] contains 10 more species than A305, and this difference comes from 5 extra nitrogen species and 5 hydrocarbon species. The model of Xu et al. [31] has the largest NH_3 submechanism, as it is in fact a detailed H/N/O mechanism [56] with one modified reaction. In turn, the size of the NH_3 submechanism of Wang et al. [32] is comparable to A305 (in terms of species). The main difference between A305 and [32] comes from the C/H/N/O submechanism. The model [32] was developed to predict, among other things, emissions of HCN, and preserving the cyanide submechanism came at a cost of 10 extra species and 121 extra reactions. In the present work, it was observed that in addition to emission formation, the cyanide pathway that starts with formation of methylamine

$$CH3 + NH_2 (+M) = CH_3NH_2 (+M), \quad (R10)$$

Table 4
Composition of the NH_3/n-heptane reduced models.

mech.	species[1]					reactions[1,2]		
	total	H/O	N/H/O	C/H/O	C/H/N/O	total	H/O + C/H/O	C/H/N/O
Thorsen[3] [37]	1365	9[4]	23	1257	75	6310	5322	792
A305	**57**	**8**	**16**	**33**	**0**	**159**	**96**	**9**
Xu [31]	67	8	21	38	0	387	207	0
Wang [32]	72	8	17	37	10	495	185	156
Liu [30]	103	8	20	75	0	572	392	0
Chang[5] [46]	47	8	N_2	38	N./A.	207	207	N./A.

[1] species Ar and He (present in some models) and their reactions are not counted.
[2] reversible reactions count as 1.
[3] detailed target mechanism for A305.
[4] O_3 not counted (no reactions).
[5] n-heptane mechanism.

plays a role in modeling IDT with reduced mechanisms, as well as nitroethane pathway via

$$C_2H_5 + NO_2 = C_2H_5NO_2 \quad (R11)$$

Larger mechanisms generated by the ACR method did contain the corresponding pathways. In smaller mechanisms, including the selected candidate, the (inhibiting) effect of these pathways is compensated by absence of some other (accelerating) pathways.

Despite that A305 does not contain any C/N species, interaction reactions between C and N species play a major role through H- and O-atom exchange reactions. The most important is H-abstraction from n-heptane by NH_2 (R4). The A305 mechanism also contains four other H-abstraction reactions by NH_2, two reactions of NO_2 and reactions (R2, R7) of CO and N_2O/NO_2 discussed in Section 3.3. This sums up to 9 reactions in the C/H/N/O subset, compared to 156 in Wang et al. [32], of which 35 are unrelated to the cyanide subset.

3.2. Performance of the mechanism

3.2.1. Ignition

Fig. 5 presents IDT of mixtures of NH_3 and n-heptane with varied percentage of n-heptane in the panels: 0 %, 0.5 %, 2 %, 10 %, 40 % and 100 % by mole. In this figure, pressure and ϕ are fixed at 100 atm and 1.0, respectively, as it is sufficient to illustrate all observed trends. Data for the complete target space (see Table 2) are reported in the SM (Figs. S8-S14). The current mechanism is compared to its target [37] and the reduced mechanisms of Xu et al. [31] and Wang et al. [32]. The mechanism of Liu et al. [30] was not considered due to its large size compared to other models (see Table 4). The Dong et al. model [42] served as target in development of [32] and is therefore included in figures for fair comparison of [32], whereas the mechanism of Xu et al. [31] did not have a target mechanism. It should be noted here that the A305 is considerably more compact than the other two mechanisms (see Table 4).

The present mechanism closely follows its target [37], except for the low-temperature region for mixtures with lowest n-heptane content: 0 % and 0.5 % (Fig. 5a,b). The performance of the Wang et al. [32] mechanism compared to its target [42] is better for neat NH_3 and similarly mediocre for the 0.5 % mixture, but in the 2 % mixture it has large deviations from both detailed models. The mechanism of Xu et al. [31] is qualitatively different to the rest, as it predicts no NTC in the 0.5 % and the 2 % n-heptane cases. In addition to that, it deviates from the other models for the 10 % n-heptane mixture in the low-temperature region. These trends are similar for mixtures at other equivalence ratios and slightly different at lower pressures, see Fig. S8 in the SM.

Overall, the present mechanism and Wang et al. [32] can be viewed comparable in terms of ignition performance, while Xu et al. [31] fails to reproduce all conditions in the selected space, most probably [37], due to absence of C-N interactions, which the two other reduced mechanism do contain. As for the Wang et al. model [32], its overall accuracy against the target [42] (calculated in the same space) is equal to 83 % suggesting that mixtures with very low n-heptane content were outside the target space of Wang et al. [32].

This, again, illustrates the fact that reduced mechanisms should not be used outside of their target spaces. Diesel fuel has a much higher energy density than NH_3. Even for n-heptane, a small amount of it enhances ignition properties of NH_3 by an order of magnitude, therefore to correctly capture ignition in non-uniformly mixed environments, low-percentage n-heptane mixtures have to be taken into account.

3.2.2. Laminar flames

For the 1D free-propagating flames, the reduction space included LBV and NO and N_2O profiles in mixtures of NH_3 + air, n-heptane + air, and 50/50 NH_3/n-heptane + air. For validation, mixtures with other compositions were analyzed as well, and the results can be found in the SM (Fig. S9).

Fig. 6a shows LBV of NH_3/air mixtures at T = 500 K and pressures of 10 and 100 atm. While good performance of all versions of the present mechanism was observed at 100 atm, the 10 atm, 100 % NH_3 case is where deviations between its intermediate version and the target were maximal (see Fig. S9(a,c) in the SM)A sensitivity analysis for LBV has shown that insertion of the terminating channel (R6) resolves the disagreement, so A305 closely follows the target at both pressures (Fig. 6a). The influence of this high-temperature biradical reaction (R6) is limited to flames at lower pressures and with high NH_3 content. All other flames analyzed in this study are unaffected by (R6).

For NH_3-air flames of Fig. 6a, the mechanism of Wang et al. [32] closely follows its target [42]. The situation is different when n-heptane is either a sole fuel or is in 50/50 proportion with NH_3 (Fig. 6b). There the present mechanism is closer to target, than Wang et al. [32], especially in rich mixtures. However, the differences between the two reduced mechanisms and their respective targets are on the same level or less than the difference in prediction between the two detailed mechanisms of Thorsen et al. [37] and Dong et al. [42], disallowing direct comparison of the two reduced mechanisms. Same (as for [32]) can be said about the mechanism of Xu et al. [31]. As discussed above, for LBV, direct interactions between hydrocarbon and nitrogen-containing species are of low importance. Only a few reactions of NO, NH_2 or NO_2 with hydrocarbon species have appeared in the LBV sensitivity analysis performed for Thorsen et al. [37] mechanism and conditions of Fig. 6b, but their importance can be concluded to be negligible.

Fig. 7 presents maximal mole fractions of N_2O and NO for two NH3/n-heptane mixtures with 50/50 (top) and 90/10 (bottom) composition at T = 500 K and p = 75 atm, while all other validation conditions can be found in the SM. While for the case of N_2O the maximal mole fractions are always located at the flame front, for $\phi \leq 0.9$ in the 50/50 mixture (Fig. 7c) and $\phi \leq 0.8$ in the 90/10 mixture (Fig. 7d), NO formation continues in the post-flame zone, for these conditions, maximal values at the flame front are plotted.

Here, the present mechanism predicts N_2O very close to the target, while for NO there are small deviations near stoichiometric mixtures. However, post-flame NO is reproduced correctly (see NO values at 1 cm above the flame in Fig. 7). The mechanism of Wang et al. [32] reproduces maximal NO concentrations perfectly, while predictions of N_2O in the 50/50 mixture (Fig. 7a) are less satisfactory. The mechanism of Xu et al. [31] is not able to predict N_2O, with the largest discrepancies to both detailed models in lean mixtures. It has to be again noted that prediction of NO in rich flames of pure n-heptane is outside the validation range of the present mechanism, and none of the tested reduced mechanisms were able to reproduce NO there (see Fig. S13 in SM).

3.2.3. Laminar flow reactors

Formation of N_2O in IC engines via the $DeNO_x$ mechanism was represented by oxidation of NH_3 in presence of NO in homogeneous constant-pressure reactors, a common configuration in kinetic studies utilized to simulate flow reactor experiments. The main difference of the simulations presented below to real flow reactors is the level of dilution. As the goal of the present study is to reproduce conditions most relevant to IC engines, it is reasonable to investigate undiluted NH_3/NO/air mixtures. At the same time, the proportions in which the unreacted NH_3/air mixture is mixed with the hot product gas (source of NO) are unknown, for that reason, in the simulations, amount of N_2 in the O_2/N_2 oxidizer mixture varied in a series: 79 %, 89.5 %, 95 %, 99 %. The first percentage corresponds to a hypothetical region with only a trace amount of product gas, the second - to a case where NH_3/air mixture and product gas are mixed in approximately equal proportions. The 1/99 O_2/N_2 resembles a "real" flow reactor case. Due to lower dilution levels, and therefore, a non-negligible heat release, an adiabatic condition was used rather than an isothermal one. A single end time of 0.1 s was selected, as discussed in Section 2. This parameter was varied in the

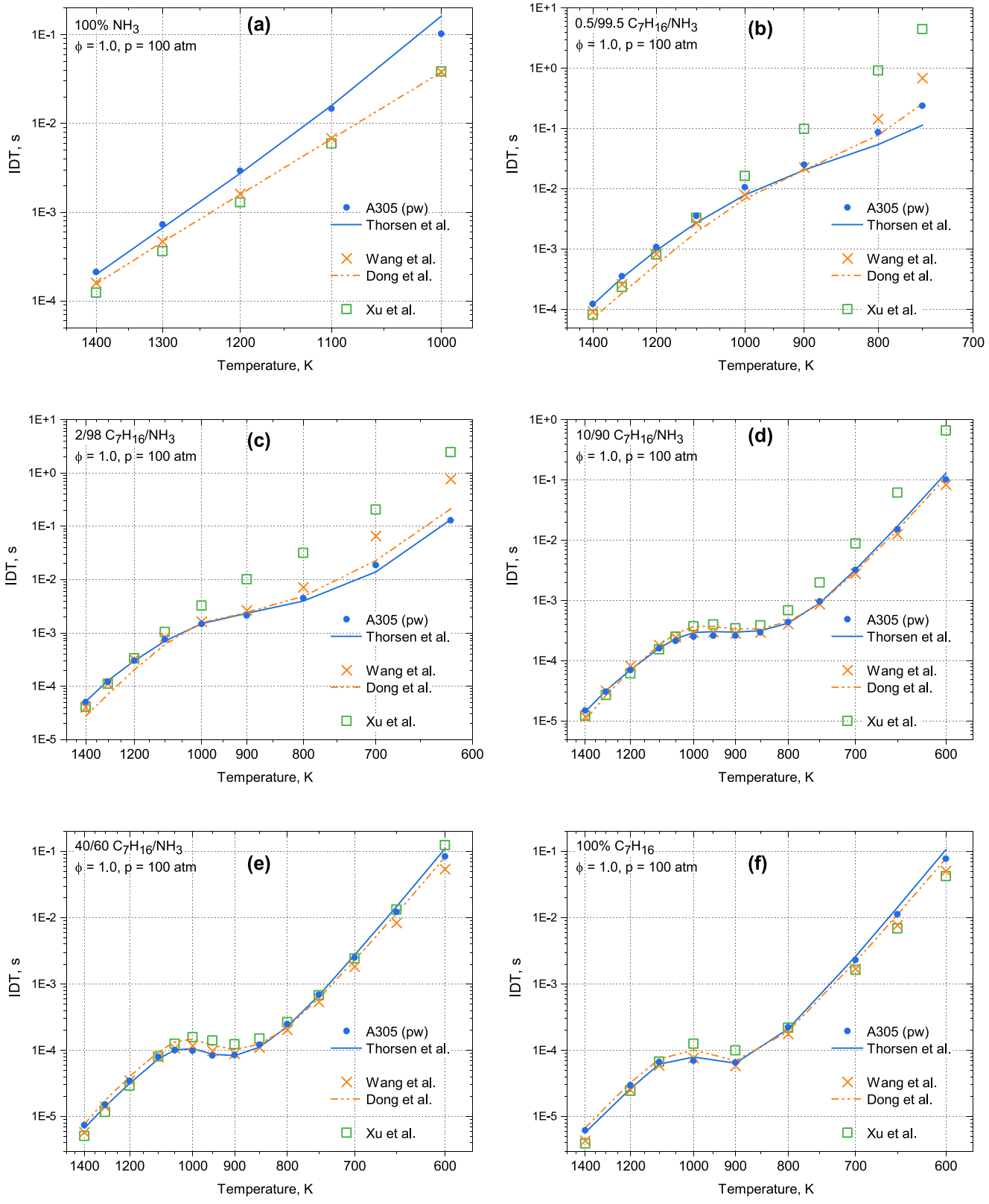

Fig. 5. IDT of NH_3/n-heptane mixtures of variable NH_3 molar percentage: 100 % (a), 99.5 % (b), 98 % (c), 90 % (d), 60 % (e) and 0 % (f) at 100 atm and $\phi = 1.0$; calculated with the present mechanism (blue dots) and its target [37] (solid lines); Wang et al. [32] (crosses) and its target [42] (dash-dot lines), and Xu et al. [31] (squares). (For interpretation of the references to colour in this figure legend, the reader is referred to the web version of this article.)

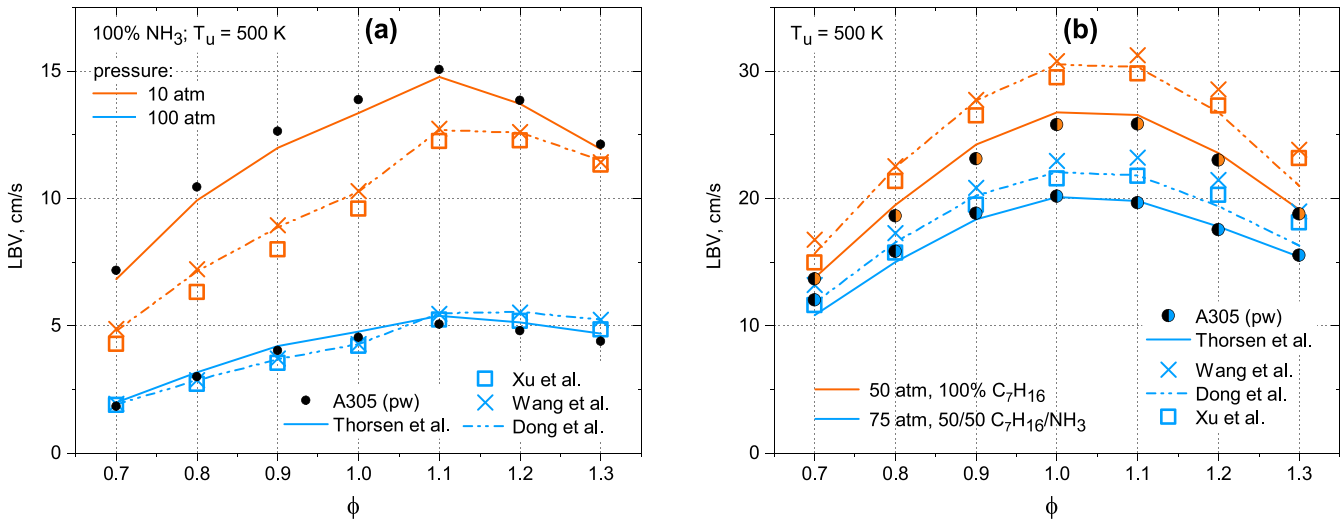

Fig. 6. LBV of NH_3/n-heptane at different pressures: 100 % NH_3 at 10 and 100 atm (a); 100 % n-heptane at 50 atm and 50/50 mixture (by mole) at 75 atm (b); calculated with the present mechanism (black dots) and its target [37] (solid lines); Wang et al. [32] (crosses) and its target [42] (dash-dot lines), and Xu et al. [31] (squares).

preliminary analysis, and it was concluded that with the selected time, all trends are captured. In this section, the results are presented as N_2O mole fractions at the end time of 0.1 s, plotted as a function of initial reactor temperature.

Fig. 8 shows selected plots of N_2O mole fraction at 0.1 s as function of initial temperature for two mixtures: with 10.5/90.5 O_2/N_2 ratio and $\phi = 0.6$ (top); and 1/99 O_2/N_2 with $\phi = 1.0$ (bottom), while other results are reported in SM (Fig. S14). The effect of pressure is illustrated by left (10 atm) and right columns (100 atm). With rising pressure, N_2O formation increases, and the $DeNO_x$ temperature window shifts to lower temperatures. An exactly opposite trend is observed when increasing dilution. Rapid drop of N_2O at higher temperatures corresponds to autoignition occurring at 0.1 s. To illustrate how much initial presence of NO affects formation of N_2O, Fig. 8a shows a case calculated for the same mixture in which NO is replaced by N_2. The difference is of about orders of magnitude at lower temperatures, while closer to 0.1 s ignition temperatures, more of NO_2, necessary for N_2O production via low-temperature pathway [2].

$$NH_2 + NO_2 = N_2O + H_2O, \quad \text{(R12)}$$

is formed from NH_3 rather than from NO.

The two reduced mechanisms, of the present work and Wang et al. [32], represent their respective target mechanisms well, except for a case of 10/90 O_2/N_2 at 100 atm, where the present mechanism deviates by about 25 K in predicting the sharp rise in N_2O formation. The mechanisms of Xu et al. [31] and the parent of its NH_3 submechanism, the detailed mechanism of Bertolino et al. [56], differ in only one reaction in the NH_3 submechanism (and H2 submodel in [31] is from [46]), therefore, their predictions are almost identical to each other. However, compared to the rest, they show highest amounts of N_2O at most conditions.

For these $NH_3/O_2/NO$ oxidation cases, major differences are observed between the detailed models: Thorsen et al. [37], Dong et al. [42] and Bertolino et al. [56]. This is best seen in Fig. 8a, where at ca. 1125 K Dong et al. predicts twice as much N_2O as Thorsen et al., and Bertolino et al. predicts twice as much N_2O as Dong et al. Reaction analysis has revealed that all difference at this temperature is due to selection of the two rate constants of the key channels

$$NH_2 + HO_2 = NH_3 + O_2 \quad \text{(R13)}$$

$$NH_2 + HO_2 = H_2NO + OH, \quad \text{(R14)}$$

of which the latter is chain-propagating and the former is chain-terminating [57]. Thorsen et al. [37] rely on recent calculations of Klippenstein and Glarborg [57], who predict the termination channel to be about 3–3.5 times faster than propagating in the temperature window of Fig. 8. Dong et al. [42] consider calculations of Stagni et al. [58] for the reverse reaction of (R13), i.e.:

$$NH_3 + O_2 = NH_2 + HO_2 \quad \text{(-R13)}$$

When reverted, the rate constant [58] becomes practically identical to Klippenstein and Glarborg inside the considered temperature window. For the H_2NO channel, Dong et al. follow Stagni et al. [58] who use recommendations of Baulch et al. [59]. However, Baulch et al. [59] provided value for the ***total*** rate constant of $NH_2 + HO_2$, which at that time was believed to have $H_2NO + OH$ as the dominant channel. So, when two channels in Stagni et al. are added together, the total rate becomes twice as high as recommended by Baulch et al. Finally, Bertolino et al. optimized Stagni et al. mechanism, and the H_2NO channel has received even higher rate (by a factor of 1.5). Fig. S5 in the SM illustrates differences in the rate constants for (R13, R14).

When Klippenstein and Glarborg [57] values are substituted into the mechanisms of Dong et al. and Bertolino et al., the predictions of all mechanisms for the conditions of Fig. 8a become much closer to each other (see Fig. S5 in the SM). Discrepancies at other pressures and temperatures still exist, however, the purpose of this subsection is not to perform an analysis of the detailed mechanisms (which is outside the scope of this work), but to highlight that selection of the detailed mechanism as a reduction target is an important step before reduction process.

3.3. *Effect of CO on N_2O formation*

In the modeling of the previous subsection, it was assumed that diluent gas consists of N_2 with presence of NO. The real product gas of NH_3/n-heptane combustion, however, will also contain CO_2, H_2O, H_2 and CO. While the main products CO_2 and H_2O can be assumed to have only a thermal effect in the considered target space, it is known that CO affects $DeNO_x$ NH_3 oxidation, and this has been subject of numerous studies, as listed in, e.g., [60]. Below, effect of CO on N_2O formation was analyzed in the same target space as in Section 3.2.3, with a constant 1 % CO added to every $NH_3/O_2/N_2/NO$ mixture.

As discussed in Section 2.4, recent literature on (R2) suggests that the value implemented in the target model [37] is most likely incorrect. Its

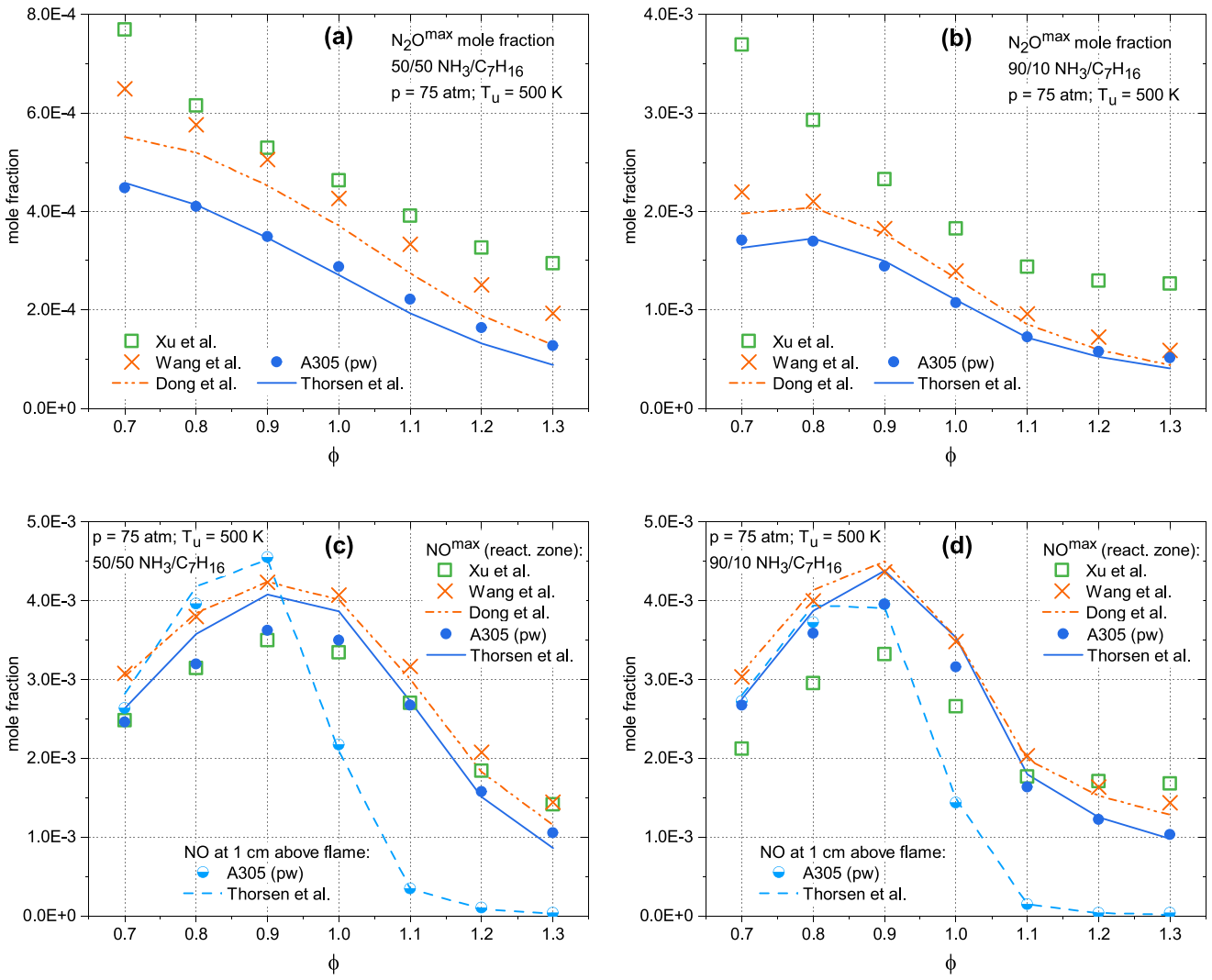

Fig. 7. Maximal (reaction zone) mole fractions of N_2O (top) and NO (bottom) for two NH_3/n-heptane mixtures with 50/50 (left) and 90/10 (right) composition at T = 500 K and 75 atm.; calculated with the present mechanism (dark-blue circles) and its target [37] (solid lines); Wang et al. [32] (crosses) and its target [42] (dash-dot lines), and Xu et al. [31] (squares). Also shown are NO at 10 mm above the flame front for present mechanism (light-blue circles) and its target [37] (dashed lines). (For interpretation of the references to colour in this figure legend, the reader is referred to the web version of this article.)

effect on DeNO$_x$ N_2O formation is illustrated in Fig. 9. Two cases are shown here, that correspond to the same conditions as Fig. 8a,d, but with additional 1 % CO. Fig. S14 in the SM covers the complete target space. In the right panel of Fig. 9, temporal N_2O profiles for the two mixtures are shown at a single T = 1150 K.

For the less diluted mixture, original rate of (R2) in [37] results in increased N_2O consumption after ca. 0.01 s (dashed blue curve in Fig. 9b), while implementation of the "slow" rate from [51] (adopted in present work) makes N_2O profile calculated with either reduced or detailed mechanism [37] comparable to a case without CO (dotted blue lines in Fig. 9a,b). Overall, end concentrations of N_2O are drastically different for all mixtures due to (R2), and literature mechanisms, either target mechanism for this work [37] or reduced model of Wang et al. [32], significantly overpredict N_2O consumption by CO.

The chemical effect of CO, however, is not only limited to the speed of (R2). This is best seen for the more diluted mixture (Fig. 9c,d) by comparing the predictions of Thorsen et al. [37] with "slow" (R2) (solid blue) and the "inert-CO" curve (dot blue). CO chemically hinders N_2O formation at the initial stage (see Fig. 9d), resulting in qualitatively different N_2O profiles. Reaction analysis has identified that a major contributing reaction is $CO + NO_2 = CO_2 + NO$ (R7) that consumes NO_2, needed for N_2O formation via (R12). This is also illustrated by comparing predictions of the reduced mechanism with (solid red) and without (dotted red) (R7). Some disagreement still exists between the present mechanism (solid red) and [37] with "slow" (R2) (solid blue), however, addition of extra species, e.g., HNCO and NCO, was found to be necessary for improvement, which was considered impractical. In addition to oxidation, some differences due to (R2) were observed in the predicted N_2O profiles before ignition of NH_3/n-heptane mixtures (see Fig. S15 in SM).

In this subsection two things were highlighted. First, available detailed and reduced models might underpredict N_2O concentrations if mixtures containing CO are considered. Second, even though the effect of CO might not be as dramatic as literature models predict, it might still be insufficient to completely omit all chemical interactions between nitrogen-containing species and CO in the reduced models.

4. Conclusions

A new reduced mechanism is developed for use in simulations of NH_3 combustion in dual-fuel IC engines. The target space for reduction (see Table 2) has been identified after a review of experimental studies of NH_3 engines, to the authors knowledge including all published work on this topic up until mid 2023. Diesel was found to be the most common

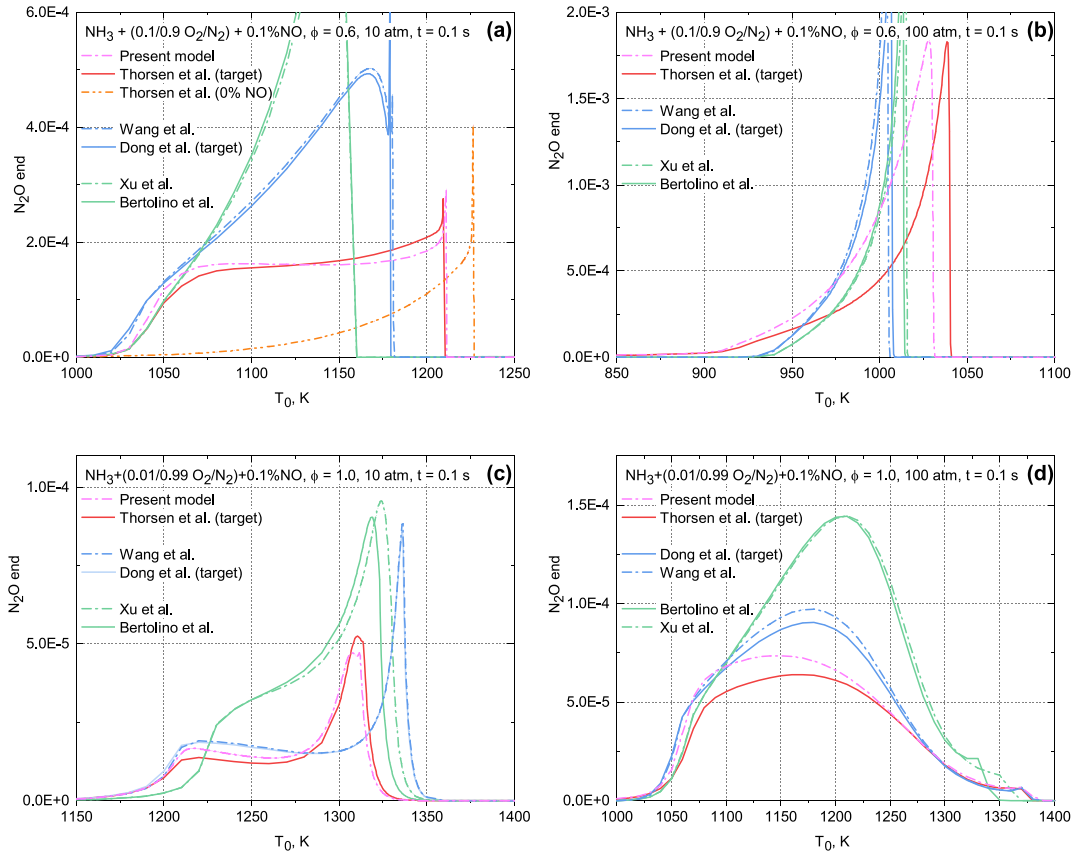

Fig. 8. N_2O end concentrations (at 0.1 s) vs. initial temperature for mixtures of 10.5/90.5 O_2/N_2 ratio with $\phi = 0.6$ (top), and 1/99 O_2/N_2 with $\phi = 1.0$ (bottom). Pressures are 10 atm (left) and 100 atm (right). Solid lines: detailed (target) mechanisms, dash-dot: reduced mechanisms, dash-dot-dot: no initial presence of NO.

secondary component of the dual fuel, which was approximated by n-heptane in the present work. The considered space for reduction included 626 combustion cases that covered ignition, flames and oxidation of NH_3/n-heptane mixtures, and they were simulated in real time during reduction. Particularly, mixtures with very low molar percentage of n-heptane were considered, which have been observed to have a distinct ignition behavior and are very important for the applications since the pilot fuel is expected to be included in small proportion. Emission of N_2O, a strong greenhouse gas, was also targeted. The modeled combustion and oxidation cases were constructed with the goal to preserve the ability of the mechanism to capture formation of N_2O via two possible routes advocated for in the experimental studies, i.e., the disrupted flame mechanism and the DeNOx mechanism, occurring when unburned NH_3 reacts with NO in product gas.

A recently published detailed mechanism [37] has served as target for reduction, and a semi-detailed base mechanism with subsets from [32,46] was constructed prior to reduction. The ant-colony reduction methodology [33] has been utilized, combined with differential evolution optimization [33] and a sequence of manual steps. The resulting reduced mechanism contains 57 species and 159 reactions (146 reversible and 13 irreversible) and is smaller than NH_3/n-heptane mechanisms available in literature, especially in terms of reactions. However, it was found that in the considered target space the present mechanism performs as good as the larger models.

The applicability range of the mechanism corresponds to the conditions listed in Table 2, e.g. range of pressures 10–100 atm, 0–100 % NH_3 in the fuel mixture. The mechanism is supposed to be used under this conditions.

The present analysis show that inclusion of interaction reactions between carbon- and nitrogen-containing species is necessary for adequate reproduction of combustion of mixtures of NH_3 and n-heptane. At the same time, it was found to be possible to remove all reaction chain involving species containing both carbon and nitrogen atoms.

It has been observed that differences in predictions between NH_3/n-heptane reduced mechanisms are often caused by selection of rate constants of key reactions in the corresponding detailed mechanisms, highlighting the importance of relying on recent data for these rate constants.

Following the analysis of the influence of CO on N_2O formation during oxidation of NH_3 in presence of NO, performed in the present work, one reaction rate (R2) in [37], which significantly affected the results, has been replaced. This has been done by revisiting available data on the rate constant of (R2). It has been concluded that CO might have an effect on post-flame N_2O consumption, however, it is not as large as predicted by available models.

The results have indicated that post-flame oxidation of NH_3 might play a role in formation of N_2O. For that reason, if these effects are to be captured in CFD simulations of NH_3 engines, the implemented simulation approach has to consider occurrence of chemical reactions outside flame areas.

CRediT authorship contribution statement

Vladimir A. Alekseev: Writing – original draft, Visualization, Validation, Methodology, Investigation, Formal analysis, Conceptualization. **Elna J.K. Nilsson:** Writing – review & editing, Supervision, Project administration, Methodology, Funding acquisition, Conceptualization.

Declaration of competing interest

The authors declare that they have no known competing financial interests or personal relationships that could have appeared to influence

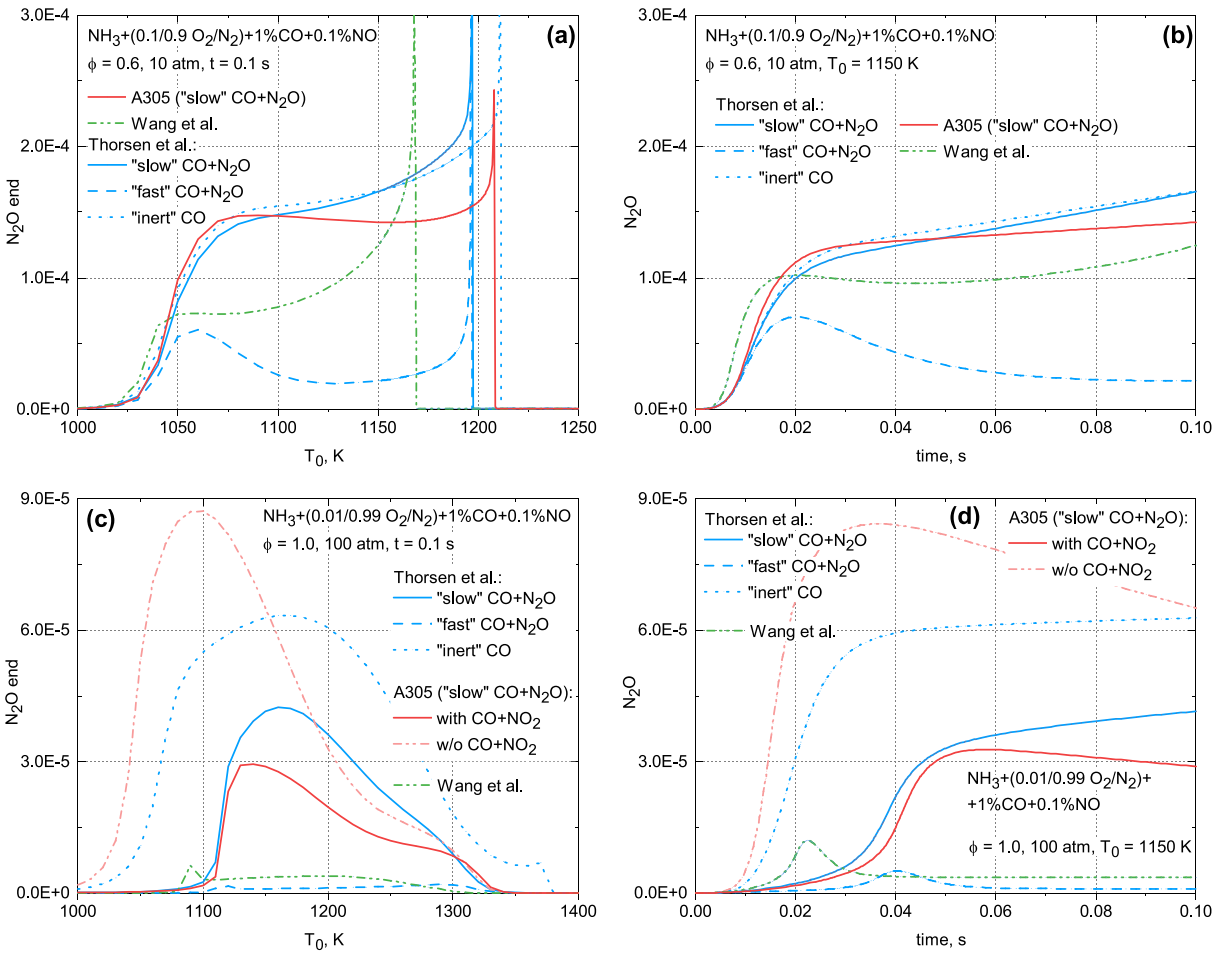

Fig. 9. N_2O end concentrations (at 0.1 s) vs. initial temperature (left), and temporal N_2O profiles at T = 1150 K (right) for two initial mixtures of Fig. 8a (top) and Fig. 8d (bottom) with additional 1 % CO (by mole). The present mechanism A305 (solid red) is compared to its target [37] with a modified "slow" (R26) (solid blue). Also shown are: A305 w/o (R7) (dash-dot red), unmodified [37] (dashed blue), [37] with chemically inert CO (dot blue), and Wang et al. [32]. (For interpretation of the references to colour in this figure legend, the reader is referred to the web version of this article.)

the work reported in this paper.

Data availability

No data was used for the research described in the article.

Acknowledgements

The authors would like to acknowledge that their contribution is part of the project ENGIMMONIA that has received funding from the European Research Council (ERC) under the European Union's Horizon 2020 research and innovation program (Grant agreement No. 955413). The authors would like to thank Professor Alexander Konnov from Lund University and Professor Peter Glarborg from the Technical University of Denmark for valuable input and discussions.

Appendix A. Supplementary material

Supplementary data to this article can be found online at https://doi.org/10.1016/j.fuel.2024.131464.

References

[1] Valera-Medina A, Xiao H, Owen-Jones M, David WIF, Bowen PJ. Ammonia for power. Prog Energ Combust Sci 2018;69:63–102. https://doi.org/10.1016/j.pecs.2018.07.001.

[2] Glarborg P, Miller JA, Ruscic B, Klippenstein SJ. Modeling nitrogen chemistry in combustion. Prog Energ Combust Sci 2018;67:31–68. https://doi.org/10.1016/j.pecs.2018.01.002.

[3] Valera-Medina A, Amer-Hatem F, Azad AK, Dedoussi IC, de Joannon M, Fernandes RX, et al. Review on ammonia as a potential fuel: from synthesis to economics. Energy Fuels 2021;35(9):6964–7029. https://doi.org/10.1021/acs.energyfuels.0c03685.

[4] Chiong M-C, Chong CT, Ng J-H, Mashruk S, Chong WWF, Samiran NA, et al. Advancements of combustion technologies in the ammonia-fuelled engines. Energy Convers Manag 2021;244:114460. https://doi.org/10.1016/j.enconman.2021.114460.

[5] Mounaïm-Rousselle C, Mercier A, Brequigny P, Dumand C, Bouriot J, Houillé S. Performance of ammonia fuel in a spark assisted compression ignition engine. Int J Engine Res 2021;23(5):781–92. https://doi.org/10.1177/14680874211038726.

[6] Liu Z, Zhou L, Wei H. Experimental investigation on the performance of pure ammonia engine based on reactivity controlled turbulent jet ignition. Fuel 2023;335:127116. https://doi.org/10.1016/j.fuel.2022.127116.

[7] Westlye FR, Ivarsson A, Schramm J. Experimental investigation of nitrogen based emissions from an ammonia fueled SI-engine. Fuel 2013;111:239–47. https://doi.org/10.1016/j.fuel.2013.03.055.

[8] Lhuillier C, Brequigny P, Contino F, Mounaïm-Rousselle C. Experimental study on ammonia/hydrogen/air combustion in spark ignition engine conditions. Fuel 2020;269:117448. https://doi.org/10.1016/j.fuel.2020.117448.

[9] Pandey JK, Dinesh MH, Kumar GN. A comparative study of NOx mitigating techniques EGR and spark delay on combustion and NOx emission of ammonia/hydrogen and hydrogen fuelled SI engine. Energy 2023;276:127611. https://doi.org/10.1016/j.energy.2023.127611.

[10] Pyrc M, Gruca M, Tutak W, Jamrozik A. Assessment of the co-combustion process of ammonia with hydrogen in a research VCR piston engine. Int J Hydrog Energy 2023;48(7):2821–34. https://doi.org/10.1016/j.ijhydene.2022.10.152.

[11] Wei W, Li G, Zhang Z, Long Y, Zhang H, Huang Y, et al. Effects of ammonia addition on the performance and emissions for a spark-ignition marine natural gas engine. Energy 2023;272:127092. https://doi.org/10.1016/j.energy.2023.127092.

[12] Oh S, Park C, Kim S, Kim Y, Choi Y, Kim C. Natural gas–ammonia dual-fuel combustion in spark-ignited engine with various air–fuel ratios and split ratios of ammonia under part load condition. Fuel 2021;290:120095. https://doi.org/10.1016/j.fuel.2020.120095.
[13] Oh S, Park C, Oh J, Kim S, Kim Y, Choi Y, et al. Combustion, emissions, and performance of natural gas–ammonia dual-fuel spark-ignited engine at full-load condition. Energy 2022;258:124837. https://doi.org/10.1016/j.energy.2022.124837.
[14] Gross CW, Kong S-C. Performance characteristics of a compression-ignition engine using direct-injection ammonia–DME mixtures. Fuel 2013;103:1069–79. https://doi.org/10.1016/j.fuel.2012.08.026.
[15] Ryu K, Zacharakis-Jutz GE, Kong S-C. Performance characteristics of compression-ignition engine using high concentration of ammonia mixed with dimethyl ether. Appl Energy 2014;113:488–99. https://doi.org/10.1016/j.apenergy.2013.07.065.
[16] Førby N, Thomsen TB, Cordtz RF, Bræstrup F, Schramm J. Ignition and combustion study of premixed ammonia using GDI pilot injection in CI engine. Fuel 2023;331:125768. https://doi.org/10.1016/j.fuel.2022.125768.
[17] Niki Y, Nitta Y, Sekiguchi H, Hirata K. Diesel fuel multiple injection effects on emission characteristics of diesel engine mixed ammonia gas into intake air. J Eng Gas Turbines Power 2019;141(6). https://doi.org/10.1115/1.4042507.
[18] Niki Y. Reductions in unburned ammonia and nitrous oxide emissions from an ammonia-assisted diesel engine with early timing diesel pilot injection. J Eng Gas Turbines Power 2021;143(9). https://doi.org/10.1115/1.4051002.
[19] Yousefi A, Guo H, Dev S, Liko B, Lafrance S. Effects of ammonia energy fraction and diesel injection timing on combustion and emissions of an ammonia/diesel dual-fuel engine. Fuel 2022;314:122723. https://doi.org/10.1016/j.fuel.2021.122723.
[20] Yousefi A, Guo H, Dev S, Lafrance S, Liko B. A study on split diesel injection on thermal efficiency and emissions of an ammonia/diesel dual-fuel engine. Fuel 2022;316:123412. https://doi.org/10.1016/j.fuel.2022.123412.
[21] Zhang Z, Long W, Dong P, Tian H, Tian J, Li B, et al. Performance characteristics of a two-stroke low speed engine applying ammonia/diesel dual direct injection strategy. Fuel 2023;332:126086. https://doi.org/10.1016/j.fuel.2022.126086.
[22] Sun W, Zeng W, Guo L, Zhang H, Yan Y, Lin S, et al. An optical study of the combustion and flame development of ammonia-diesel dual-fuel engine based on flame chemiluminescence. Fuel 2023;349:128507. https://doi.org/10.1016/j.fuel.2023.128507.
[23] Wu Y, Zhang Y, Xia C, Chinnathambi A, Nasif O, Gavurová B, et al. Assessing the effects of ammonia (NH3) as the secondary fuel on the combustion and emission characteristics with nano-additives. Fuel 2023;336:126831. https://doi.org/10.1016/j.fuel.2022.126831.
[24] Mi S, Wu H, Pei X, Liu C, Zheng L, Zhao W, et al. Potential of ammonia energy fraction and diesel pilot-injection strategy on improving combustion and emission performance in an ammonia-diesel dual fuel engine. Fuel 2023;343:127889. https://doi.org/10.1016/j.fuel.2023.127889.
[25] Jin S, Wu B, Zi Z, Yang P, Shi T, Zhang J. Effects of fuel injection strategy and ammonia energy ratio on combustion and emissions of ammonia-diesel dual-fuel engine. Fuel 2023;341:127668. https://doi.org/10.1016/j.fuel.2023.127668.
[26] Elumalai R, Ravi K. Strategy to reduce carbon emissions by adopting ammonia–Algal biodiesel in RCCI engine and optimize the fuel concoction using RSM methodology. Int J Hydrog Energy 2022;47(94):39701–18. https://doi.org/10.1016/j.ijhydene.2022.09.169.
[27] Ryu K, Zacharakis-Jutz GE, Kong S-C. Effects of gaseous ammonia direct injection on performance characteristics of a spark-ignition engine. Appl Energy 2014;116:206–15. https://doi.org/10.1016/j.apenergy.2013.11.067.
[28] Liu S, Lin Z, Zhang H, Lei N, Qi Y, Wang Z. Impact of ammonia addition on knock resistance and combustion performance in a gasoline engine with high compression ratio. Energy 2023;262:125458. https://doi.org/10.1016/j.energy.2022.125458.
[29] Liu Z, Zhou L, Zhong L, Wei H. Enhanced combustion of ammonia engine based on novel air-assisted pre-chamber turbulent jet ignition. Energy Convers Manag 2023;276:116526. https://doi.org/10.1016/j.enconman.2022.116526.
[30] Liu L, Wu Y, Wang Y. Numerical investigation on the combustion and emission characteristics of ammonia in a low-speed two-stroke marine engine. Fuel 2022;314. https://doi.org/10.1016/j.fuel.2021.122727.
[31] Xu L, Chang Y, Treacy M, Zhou Y, Jia M, Bai X-S. A skeletal chemical kinetic mechanism for ammonia/n-heptane combustion. Fuel 2023;331:125830. https://doi.org/10.1016/j.fuel.2022.125830.
[32] Wang B, Dong S, Jiang Z, Gao W, Wang Z, Li J, et al. Development of a reduced chemical mechanism for ammonia/n-heptane blends. Fuel 2023;338:127358. https://doi.org/10.1016/j.fuel.2022.127358.
[33] Pichler C. Identification of principal chemical subsets of biofuel combustion: Ants walking in renewable fire. PhD thesis. Lund: Lund University; 2020:66.
[34] ANSYS Chemkin 2020 R2. ANSYS, Inc.; 2020.
[35] Christensen M, Nilsson EJK, Konnov AA. The temperature dependence of the laminar burning velocities of methyl formate+air flames. Fuel 2015;157:162–70. https://doi.org/10.1016/j.fuel.2015.04.072.
[36] Mastorakos E. Ignition of turbulent non-premixed flames. Prog Energ Combust Sci 2009;35(1):57–97. https://doi.org/10.1016/j.pecs.2008.07.002.
[37] Thorsen LS, Jensen MST, Pullich MS, Christensen JM, Hashemi H, Glarborg P, et al. High pressure oxidation of NH3/n-heptane mixtures. Combust Flame 2023;254:112785. https://doi.org/10.1016/j.combustflame.2023.112785.
[38] Lubrano Lavadera M, Han XL, Konnov AA. Comparative effect of ammonia addition on the laminar burning velocities of methane, n-heptane, and iso-octane. Energy Fuels 2021;35(9):7156–68. https://doi.org/10.1021/acs.energyfuels.0c03424.
[39] Dai LM, Gersen S, Glarborg P, Mokhov A, Levinsky H. Autoignition studies of NH3/CH4 mixtures at high pressure. Combust Flame 2020;218:19–26. https://doi.org/10.1016/j.combustflame.2020.04.020.
[40] Dai LM, Hashemi H, Glarborg P, Gersen S, Marshall P, Mokhov A, et al. Ignition delay times of NH3/DME blends at high pressure and low DME fraction: RCM experiments and simulations. Combust Flame 2021;227:120–34. https://doi.org/10.1016/j.combustflame.2020.12.048.
[41] Issayev G, Giri BR, Elbaz AM, Shrestha KP, Mauss F, Roberts WL, et al. Ignition delay time and laminar flame speed measurements of ammonia blended with dimethyl ether: a promising low carbon fuel blend. Renew Energy 2022;181:1353–70. https://doi.org/10.1016/j.renene.2021.09.117.
[42] Dong S, Wang B, Jiang Z, Li Y, Gao W, Wang Z, et al. An experimental and kinetic modeling study of ammonia/n-heptane blends. Combust Flame 2022;246:112428. https://doi.org/10.1016/j.combustflame.2022.112428.
[43] Glarborg P. The NH3/NO2/O2 system: constraining key steps in ammonia ignition and N2O formation. Combust Flame 2023;257:112311. https://doi.org/10.1016/j.combustflame.2022.112311.
[44] Zhang KW, Banyon C, Bugler J, Curran HJ, Rodriguez A, Herbinet O, et al. An updated experimental and kinetic modeling study of n-heptane oxidation. Combust Flame 2016;172:116–35. https://doi.org/10.1016/j.combustflame.2016.06.028.
[45] Yu L, Zhou W, Feng Y, Wang W, Zhu J, Qian Y, et al. The effect of ammonia addition on the low-temperature autoignition of n-heptane: an experimental and modeling study. Combust Flame 2020;217:4–11. https://doi.org/10.1016/j.combustflame.2020.03.019.
[46] Chang Y, Jia M, Wang P, Niu B, Liu J. Construction and derivation of a series of skeletal chemical mechanisms for n-alkanes with uniform and decoupling structure based on reaction rate rules. Combust Flame 2022;236:111785. https://doi.org/10.1016/j.combustflame.2021.111785.
[47] Pichler C, Nilsson EJK. Composition of reduced mechanisms for ignition of biodiesel surrogates. Fuels 2020;1(1):15–29. https://doi.org/10.3390/fuels1010003.
[48] Pichler C, Nilsson EJK. Analysis of important chemical pathways of n-heptane combustion in small skeletal mechanisms. Energy Fuels 2020;34(1):758–68. https://doi.org/10.1021/acs.energyfuels.9b03263.
[49] Goodwin DG, Moffat HK, Schoegl I, Speth RL, Weber BW. Cantera: an object-oriented software toolkit for chemical kinetics, thermodynamics, and transport processes, Version 2.4.0. 2023.
[50] The OpenFOAM Foundation, OpenFOAM; 2023. Available from: https://www.openfoam.org/.
[51] Loirat H, Caralp F, Destriau M, Lesclaux R. Oxidation of carbon monoxide by nitrous oxide between 1076 and 1228 K: determination of the rate constant of the exchange reaction. J Phys Chem 1987;91(26):6538–42. https://doi.org/10.1021/j100310a023.
[52] Lubrano Lavadera M, Brackmann C, Konnov AA. Laminar burning velocities and nitric oxide formation in premixed dimethyl ether/air flames: experiments and kinetic modeling. Combust Flame 2022;246:112411. https://doi.org/10.1016/j.combustflame.2022.112411.
[53] Tsang W, Herron JT. Chemical kinetic Data Base for propellant combustion I. reactions involving NO, NO2, HNO, HNO2, HCN and N2O. J Phys Chem Ref Data 1991;20(4):609–63. https://doi.org/10.1063/1.555890.
[54] Wang Y, Fu G, Zhang Y, Xu X, Wan H. O-atom transfer reaction from N2O to CO: a theoretical investigation. Chem Phys Lett 2009;475(4):202–7. https://doi.org/10.1016/j.cplett.2009.05.044.
[55] Krupnov AA, Pogosbekian MY. Analysis of experimental data on CO and N2O interaction with CO2 production based on the results of DFT calculations. Kinet Catal 2019;60(2):164–74. https://doi.org/10.1134/S0023158419020046.
[56] Bertolino A, Fürst M, Stagni A, Frassoldati A, Pelucchi M, Cavallotti C, et al. An evolutionary, data-driven approach for mechanism optimization: theory and application to ammonia combustion. Combust Flame 2021;229:111366. https://doi.org/10.1016/j.combustflame.2021.02.012.
[57] Klippenstein SJ, Glarborg P. Theoretical kinetics predictions for NH2 + HO2. Combust Flame 2022;236:111787. https://doi.org/10.1016/j.combustflame.2021.111787.
[58] Stagni A, Cavallotti C, Arunthanayothin S, Song Y, Herbinet O, Battin-Leclerc F, et al. An experimental, theoretical and kinetic-modeling study of the gas-phase oxidation of ammonia. React Chem Eng 2020;5(4):696–711. https://doi.org/10.1039/c9re00429g.
[59] Baulch DL, Bowman CT, Cobos CJ, Cox RA, Just T, Kerr JA, et al. Evaluated kinetic data for combustion modeling: supplement II. J Phys Chem Ref Data 2005;34(3):757–1397. https://doi.org/10.1063/1.1748524.
[60] Alzueta MU, Salas I, Hashemi H, Glarborg P. CO assisted NH3 oxidation. Combust Flame 2023;257:112438. https://doi.org/10.1016/j.combustflame.2022.112438.